Int. J. Heat Mass Transfer. Vol. 37, No. 1, pp. 139–151, 1994
Printed in Great Britain

0017–9310/94 $6.00 + 0.00

A new turbulence model for predicting fluid flow and heat transfer in separating and reattaching flows—I. Flow field calculations

K. ABE and T. KONDOH
Toyota Central Research and Development Laboratories, Inc., Nagakute-cho, Aichi-gun, Aichi-ken 480-11, Japan

and

Y. NAGANO
Department of Mechanical Engineering, Nagoya Institute of Technology, Gokiso-cho, Showa-ku, Nagoya 466, Japan

(*Received* 25 *February* 1993 *and in final form* 18 *May* 1993)

Abstract—To calculate complex turbulent flows with separation and heat transfer, we have developed a new turbulence model for flow field, which is modified from the latest low-Reynolds-number k–ε model. The main improvement is achieved by the introduction of the Kolmogorov velocity scale, $u_\varepsilon \equiv (\nu\varepsilon)^{1/4}$, instead of the friction velocity u_τ, to account for the near-wall and low-Reynolds-number effects in both attached and detached flows. The present model predicts quite successfully the separating and reattaching flows downstream of a backward-facing step, which involve most of the essential physics of complex turbulent flows, under various flow conditions. We have also discussed in detail the structure of the separating and reattaching flow based on the computational results, and presented several important features closely related to the mechanism of turbulent heat transfer.

1. INTRODUCTION

IN MANY practical applications, flows accompany separation and subsequent reattachment, which not only determine the structure of a flow field but also influence the mechanism of heat transfer. To evaluate accurately the turbulent heat transfer coefficient in separating and reattaching flows, it is indispensable to predict the turbulent flow fields with sufficient accuracy.

In most of the previous studies, the k–ε model has been used to predict separating and reattaching turbulent flows (see, for example, Launder [1]). Also, several attempts to simulate both the flow field and the heat transfer have been performed [2, 3]. Though the k–ε model is quite useful, major problems remain. For example, (1) in calculating turbulent flows with the k–ε model, the wall functions are usually employed as the boundary condition on solid walls. However, their application to recirculating regions is open to question. (2) The previous k–ε models usually give 15–20% underprediction of the flow reattachment length downstream of a backward-facing step [4, 5], which is the most fundamental quantity to be predicted in separating and reattaching flows. It is known that the accurate prediction of heat transfer in separating flows is impossible without reliable predictions of the flow in the recirculating region.

On the other hand, today's k–ε models have been significantly improved so that they may work even in the vicinity of the wall; they are called the 'low-Reynolds-number k–ε models'. Nešić and Postlethwaite [6] performed the calculation of mass transfer in a separating flow using the Lam–Bremhorst model [7] at Schmidt numbers higher than 10^3. However, as described below, the Lam–Bremhorst model gives the incorrect near-wall limiting behavior of the Reynolds stress, and hence the correct prediction of heat transfer cannot be expected in high Prandtl or Schmidt number flows. For the accurate prediction of heat transfer in high Prandtl number flows, we need to reproduce the near-wall limiting behavior correctly. Among the existing low-Reynolds-number k–ε models, the model developed by Nagano and Tagawa (hereinafter referred to as the NT model) [8, 9] is regarded as one of the most reliable. The model can reproduce the near-wall limiting behavior and provides accurate predictions for the attached turbulent flows such as channel and boundary-layer flows with favorable or adverse pressure gradients. However, since the model functions of the NT model contain the friction velocity u_τ, it breaks down around the separating and the reattaching points where $u_\tau = 0$. Thus, contrary to the real phenomena, the NT model forces the Reynolds stress to vanish there.

In this study, we propose a new k–ε model which is modified from the NT model. The principal improvement is the usage of the Kolmogorov velocity scale

NOMENCLATURE

b_{ij} anisotropic tensor, $\overline{u_i u_j}/2k - \delta_{ij}/3$
C_f mean skin friction coefficient, $\tau_w/(\rho \bar{U}_0^2/2)$, $\tau_w/(\rho \bar{U}_e^2/2)$ or $-\tau_w/(\rho \bar{U}_N^2/2)$
C_{fm} mean skin friction coefficient based on bulk velocity, $\tau_w/(\rho \bar{U}_m^2/2)$
C_f' fluctuating skin friction coefficient
C_p mean static pressure coefficient, $(\bar{p} - \bar{p}_0)/(\rho \bar{U}_0^2/2)$
C_μ, $C_{\varepsilon 1}$, $C_{\varepsilon 2}$ model constants of k–ε model
D channel width upstream of step
ER channel expansion ratio, $(D+H)/D$
f_μ, f_ε model functions of low-Reynolds-number k–ε model
H height of backward-facing step
k turbulent energy, $\overline{u_i u_i}/2$
N_ξ, N_η numbers of grid points in ξ- and η-directions, respectively
n local coordinate normal to wall surface
$\bar{p}$ mean static pressure
Re_0 Reynolds number based on channel centerline velocity, $2\bar{U}_0\delta/\nu$
Re_H Reynolds number based on step height, $\bar{U}_0 H/\nu$
Re_m Reynolds number based on channel bulk velocity, $2\bar{U}_m\delta/\nu$
Re_N Reynolds number based on maximum reverse-flow velocity, $-\bar{U}_N y_N/\nu$
$Re\theta$ Reynolds number based on momentum thickness, $\bar{U}_0\theta/\nu$
Re_τ Reynolds number based on friction velocity, $u_\tau\delta/\nu$
R_t turbulent Reynolds number, $k^2/\nu\varepsilon$
t time
$\bar{U}_i$, u_i mean velocity and turbulent fluctuation in i-direction
$\bar{U}$, $\bar{V}$, $\bar{W}$ mean velocity in x-, y- and z-directions, respectively
u, v, w turbulent fluctuation in x-, y- and z-directions, respectively
$\bar{U}_m$ bulk velocity of fully-developed channel flow
$\bar{U}^+$ nondimensional mean velocity, $\bar{U}/u_\varepsilon$
u_ε Kolmogorov velocity scale, $(\nu\varepsilon)^{1/4}$
u_τ friction velocity, $\sqrt{(\tau_w/\rho)}$
X_R flow reattachment length
x Cartesian coordinate in streamwise direction with $x = 0$ at step location
y Cartesian coordinate normal to streamwise direction with $y = 0$ at step bottom
z Cartesian coordinate in spanwise direction
y^+ nondimensional length from wall surface, $u_\tau y/\nu$
y^* nondimensional length from wall surface, $u_\varepsilon y/\nu$.

Greek symbols
δ half width of channel
δ_{ij} Kronecker delta
ε dissipation rate of turbulent energy, $\nu(\overline{\partial u_i/\partial x_j})(\overline{\partial u_i/\partial x_j})$
η generalized coordinate from lower to upper walls
θ momentum thickness
κ Von Kármán's universal constant, 0.41
ν, ν_t kinematic viscosity and eddy viscosity
ξ generalized coordinate from inlet to outlet
ρ density
σ_k, σ_ε model constants in turbulent diffusion terms of k–ε model
τ_w wall shear stress
ψ stream function.

Subscripts
e outer edge of boundary layer
i, j 1, 2 and 3 denote x-, y- and z-directions, respectively
N maximum reverse-flow point at location x
n normal direction from wall surface
R flow reattachment point
w wall surface
0 reference value at inlet to back-step channel (i.e. value at centerline in fully-developed turbulent channel inflow or value at free-stream in turbulent boundary layer inflow)
1 nearest grid point from wall surface.

$u_\varepsilon \equiv (\nu\varepsilon)^{1/4}$ instead of the friction velocity u_τ to account for the near-wall and low-Reynolds-number effects. The velocity scale u_ε becomes zero neither at the separating nor at the reattaching points in contrast to the friction velocity u_τ. Besides this major modification of the model functions, we have reevaluated the model constants in the transport equations for the turbulent energy and its dissipation rate for improvement of overall accuracy. It is shown that the separating and reattaching flows downstream of a backward-facing step are simulated quite successfully with the present model. For example, the calculated flow reattachment lengths, which have been consistently underpredicted with the previous k–ε models, are in excellent agreement with various experiments.

Furthermore, from the computational results, we have investigated the detailed structure of separating and reattaching flows and obtained several important characteristics closely related to the prediction of the heat transfer.

2. GOVERNING EQUATIONS

The governing equations to be solved are the equation of continuity, the ensemble averaged Navier–Stokes equation and the equations of the turbulent energy k and its dissipation rate ε:

$$\frac{\partial \bar{U}_i}{\partial x_i} = 0 \tag{1}$$

$$\frac{\partial \bar{U}_i}{\partial t} + \bar{U}_j \frac{\partial \bar{U}_i}{\partial x_j} = -\frac{1}{\rho}\frac{\partial \bar{p}}{\partial x_i} + \frac{\partial}{\partial x_j}\left\{\nu\left(\frac{\partial \bar{U}_i}{\partial x_j} + \frac{\partial \bar{U}_j}{\partial x_i}\right) - \overline{u_i u_j}\right\} \tag{2}$$

$$\frac{\partial k}{\partial t} + \bar{U}_j \frac{\partial k}{\partial x_j} = \frac{\partial}{\partial x_j}\left\{\left(\nu + \frac{\nu_t}{\sigma_k}\right)\frac{\partial k}{\partial x_j}\right\} - \overline{u_i u_j}\frac{\partial \bar{U}_i}{\partial x_j} - \varepsilon \tag{3}$$

$$\frac{\partial \varepsilon}{\partial t} + \bar{U}_j \frac{\partial \varepsilon}{\partial x_j} = \frac{\partial}{\partial x_j}\left\{\left(\nu + \frac{\nu_t}{\sigma_\varepsilon}\right)\frac{\partial \varepsilon}{\partial x_j}\right\} - C_{\varepsilon 1}\frac{\varepsilon}{k}\overline{u_i u_j}\frac{\partial \bar{U}_i}{\partial x_j} - C_{\varepsilon 2} f_\varepsilon \frac{\varepsilon^2}{k} \tag{4}$$

where

$$-\overline{u_i u_j} = \nu_t\left(\frac{\partial \bar{U}_i}{\partial x_j} + \frac{\partial \bar{U}_j}{\partial x_i}\right) - \frac{2}{3}k\delta_{ij} \tag{5}$$

$$\nu_t = C_\mu f_\mu \frac{k^2}{\varepsilon}. \tag{6}$$

In equations (1)–(6), f_μ and f_ε are the model functions to account for the near-wall and low-Reynolds-number effects, and C_μ, $C_{\varepsilon 1}$, $C_{\varepsilon 2}$, σ_k and σ_ε are the model constants.

3. MODIFIED LOW-REYNOLDS-NUMBER k–ε MODEL

3.1. *Original Nagano–Tagawa model*

In the original NT model, the model functions in the above equations, which are introduced to reflect the multiple length scales involved in shear flows and to satisfy the requirements for the near-wall limiting behavior of turbulence, are expressed as follows:

$$f_\mu = \left\{1 - \exp\left(-\frac{y^+}{26}\right)\right\}^2\left(1 + \frac{4.1}{R_t^{3/4}}\right) \tag{7}$$

$$f_\varepsilon = \left\{1 - \exp\left(-\frac{y^+}{6}\right)\right\}^2\left[1 - 0.3\exp\left\{-\left(\frac{R_t}{6.5}\right)^2\right\}\right] \tag{8}$$

where $y^+ = u_\tau y/\nu$ and $R_t = k^2/\nu\varepsilon$. The model constants in equations (3)–(6) are given as follows:

$$C_\mu = 0.09, \quad \sigma_k = 1.4, \quad \sigma_\varepsilon = 1.3,$$
$$C_{\varepsilon 1} = 1.45, \quad C_{\varepsilon 2} = 1.9. \tag{9}$$

This model can reproduce the near-wall asymptotic relations of $-\overline{uv} \propto y^3$, $k \propto y^2$ and $\varepsilon \propto y^0$ quite correctly [8, 9], and can predict, with very high accuracy, the attached turbulent flows with favorable or adverse pressure gradient [8, 9].

However, equations (7) and (8) contain the friction velocity u_τ. Thus, if we apply this model to separating flows, it will collapse at a separation point ($u_\tau = 0$) and also at a reattaching location ($u_\tau = 0$).

3.2. *Modification of model functions*

A new velocity scale which replaces the friction velocity u_τ is required so that the NT model can be applied to separating and reattaching flows.

In selecting a new velocity scale, we must satisfy the following essential requirements from the standpoint of turbulence modeling.

1. The velocity scale is composed of the characteristic quantities of a turbulent flow.
2. The velocity scale has no singularity at a separating or reattaching point.
3. The new model functions should reproduce the near-wall limiting behavior as correctly as the original NT model. In other words, the selected velocity scale has a finite value at the wall surface.

In what follows, we evaluate the near-wall limiting behavior of the velocity. Each component of the velocity can be expanded in terms of y near the wall as follows:

$$\begin{aligned}
\bar{U} &= \overline{A_1}y + \overline{A_2}y^2 + \overline{A_3}y^3 + \ldots, \\
\bar{V} &= \overline{B_2}y^2 + \overline{B_3}y^3 + \ldots, \\
\bar{W} &= \overline{C_1}y + \overline{C_2}y^2 + \overline{C_3}y^3 + \ldots, \\
u &= a_1 y + a_2 y^2 + a_3 y^3 + \ldots, \\
v &= b_2 y^2 + b_3 y^3 + \ldots, \\
w &= c_1 y + c_2 y^2 + c_3 y^3 + \ldots,
\end{aligned} \tag{10}$$

where y is the distance from the wall surface and an overbar ($\bar{}$) denotes the ensemble-averaged values. The friction velocity u_τ is expressed as $u_\tau = \sqrt{(\tau_w/\rho)}$, where $\tau_w = \rho\nu(\partial \bar{U}/\partial y)_w = \rho\nu\overline{A_1}$. The singularity at a separating or reattaching point occurs in the NT model because the velocity scale is determined by the mean velocity component, i.e. $u_\tau = (\nu\overline{A_1})^{1/2}$. It may be expected that, if we determine the velocity scale by the characteristic value of turbulence, the above singularity can be removed.

The obvious velocity scale of turbulence is $\sqrt{k}$, which has been most commonly used in various turbulence models (e.g. Lam and Bremhorst [7]). Recently, Zhang and Sousa [10] proposed the modification of the Nagano–Hishida model [11] with the velocity scale replaced by $\sqrt{k}$.

Though the models of Lam–Bremhorst and Zhang–Sousa can avoid the singularity, their crucial weakness is that the resultant solutions violate the proper near-

wall limiting behavior. From equation (10), the turbulence energy is expressed as follows:

$$k = \tfrac{1}{2}(a_1^2 + c_1^2)\, y^2 + \ldots \tag{11}$$

The above equation indicates that $\sqrt{k}$ changes linearly with y. Thus, the Reynolds stress $-uv$ is proportional to y^4 in the Lam–Bremhorst model, and y^7 in the Zhang–Sousa model, both of which conflict with the correct behavior $-uv \propto y^3$. For the accurate prediction of heat transfer in high Prandtl number fluids, it is extremely important to reproduce the near-wall limiting behavior correctly.

As seen from equations (10) and (11), $\sqrt{k}$ represents the fluctuating velocity itself, and has no direct relevance to the friction velocity u_τ. Hence, the choice of $\sqrt{k}$ instead of u_τ is not reasonable. It is more desirable that a new velocity scale couples in some physical manner with the fluctuation of the instantaneous friction velocity $u_\tau(t)$. The intensity of the fluctuation of the instantaneous wall shear stress $\tau_w(t)$ is expressed as follows:

$$\rho\nu\sqrt{\left\{\left(\frac{\partial u}{\partial y}\right)_w^2\right\}} = \rho\nu\sqrt{a_1^2}. \tag{12}$$

On the other hand, the dissipation ε near the wall surface is expressed as follows:

$$\varepsilon = \nu\left\{\left(\frac{\partial u}{\partial y}\right)^2 + \left(\frac{\partial v}{\partial y}\right)^2 + \left(\frac{\partial w}{\partial y}\right)^2\right\} = \nu(a_1^2 + c_1^2) + \ldots. \tag{13}$$

From equations (12) and (13), we can recognize that the Kolmogorov velocity scale $u_\varepsilon = (\nu\varepsilon)^{1/4} \simeq \{\nu\sqrt{(a_1^2 + c_1^2)}\}^{1/2}$ is closely related to the measure of the fluctuating friction velocity $\{\nu\sqrt{(a_1^2)}\}^{1/2}$. Furthermore, from equation (13), the Kolmogorov velocity scale u_ε has a finite value $\{\nu\sqrt{(a_1^2 + c_1^2)}\}^{1/2}$ on the wall surface, thus satisfying the necessary condition to reproduce the near-wall limiting behavior $-uv \propto y^3$.

Accordingly, it is legitimate to introduce the velocity scale $u_\varepsilon = (\nu\varepsilon)^{1/4}$ instead of the friction velocity u_τ. And the model functions may be written as:

$$f_\mu = \left\{1 - \exp\left(-\frac{y^*}{14}\right)\right\}^2\left[1 + \frac{5}{R_t^{3/4}}\exp\left\{-\left(\frac{R_t}{200}\right)^2\right\}\right] \tag{14}$$

$$f_\varepsilon = \left\{1 - \exp\left(-\frac{y^*}{3.1}\right)\right\}^2\left[1 - 0.3\exp\left\{-\left(\frac{R_t}{6.5}\right)^2\right\}\right] \tag{15}$$

where $y^* = u_\varepsilon y/\nu$.

On the other hand, previous studies with the standard k–ε model have suffered from the fact that the reattachment lengths of the back-step flow were always underpredicted by 15–20% compared with the experiments. One of the reasons for these underpredictions is that the wall functions have usually been employed even in the separating region. But another reason might be that the values of the model constants used are not suitable. Thus, we have reevaluated the model constants of equations (3)–(6). First, C_μ is set to a standard value of 0.09, because the structure parameter $-uv/k$ in separating flows is nearly identical with that in attached flows [12]. Next, $C_{\varepsilon 2}$ is determined to be 1.9 because free turbulent flows are well reproduced by using the typical value of $C_{\varepsilon 2} = 1.9$ along with the function $[1 - 0.3\exp\{-(R_t/6.5)^2\}]$ in f_ε as shown in the NT model [8, 9].

The other constants to be determined are $C_{\varepsilon 1}$, σ_k and σ_ε. In wall-turbulent flows, $C_{\varepsilon 1}$, $C_{\varepsilon 2}$ and σ_ε must satisfy the following relation:

$$C_{\varepsilon 1} = C_{\varepsilon 2} - \frac{\kappa^2}{\sigma_\varepsilon\sqrt{C_\mu}}. \tag{16}$$

We have investigated the effect of the model constants on the computational results, and found that the reattachment length of a backward-facing step flow is sensitive to a value of $C_{\varepsilon 1}$. The reattachment length changes by about 0.2 step height with the $C_{\varepsilon 1}$ variation of 0.01. Based on the reassessment, $C_{\varepsilon 1}$ is determined to be 1.5 as a most appropriate value, and σ_ε is put at 1.4 so that equation (16) may be satisfied. Finally, following the lead of Nagano *et al.* [8, 9] that the correct profile of the eddy viscosity in internal flows can be obtained by setting $\sigma_k \simeq \sigma_\varepsilon$, σ_k is assigned to 1.4, which is the same value as in the NT model. In sum, the present new model uses the following set of model constants:

$$C_\mu = 0.09, \quad \sigma_k = 1.4, \quad \sigma_\varepsilon = 1.4,$$
$$C_{\varepsilon 1} = 1.5, \quad C_{\varepsilon 2} = 1.9. \tag{17}$$

4. MODEL ASSESSMENT IN ATTACHED TURBULENT FLOWS

In our new proposal, we have modified not only the model functions but some model constants of the original NT model. Thus, to confirm the basic accuracy of the present model, we have applied it to the predictions of the representative attached turbulent flows, i.e. a fully developed channel flow and a boundary layer flow with an adverse pressure gradient. The latter is known to be difficult to predict accurately with the previous k–ε models [8, 9].

The distributions of the velocity and the eddy viscosity obtained from the present model are compared with the direct simulation data (DNS) [13] in Fig. 1. For both the velocity and the eddy viscosity, the present predictions show good agreement with the DNS data. In Fig. 2, the computational results for the skin friction coefficient at various Reynolds numbers are shown. It can be seen that the present model predicts accurately the Reynolds-number dependence in a fully turbulent regime, and for the Reynolds number less than 10^4 the model reflects reasonably the low-Reynolds-number effect. The almost perfect agreement in both skin friction coefficients in Figs. 2(a) and (b)

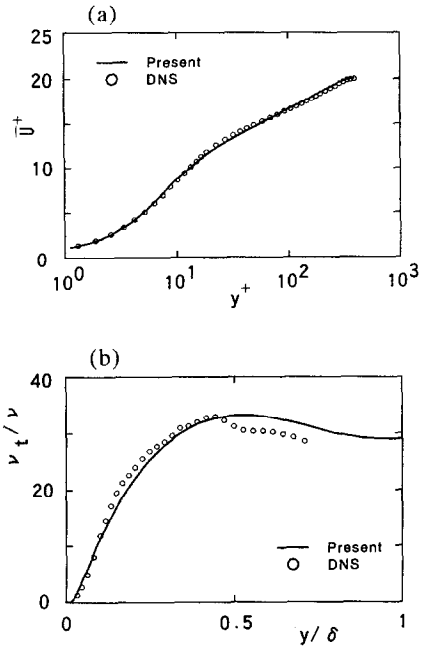

FIG. 1. Comparison of channel flow predictions with DNS data ($Re_\tau = 395$): (a) mean velocity; (b) eddy viscosity.

indicates that the model captures accurately the Reynolds-number dependence of the wall shear-stress and the ratio of the centerline velocity $\bar{U}_0$ to the mean bulk velocity $\bar{U}_m$. These features pertaining to the Reynolds-number effects may be quite advantageous in the model application to more complex turbulent flows.

The calculation of an adverse pressure gradient flow

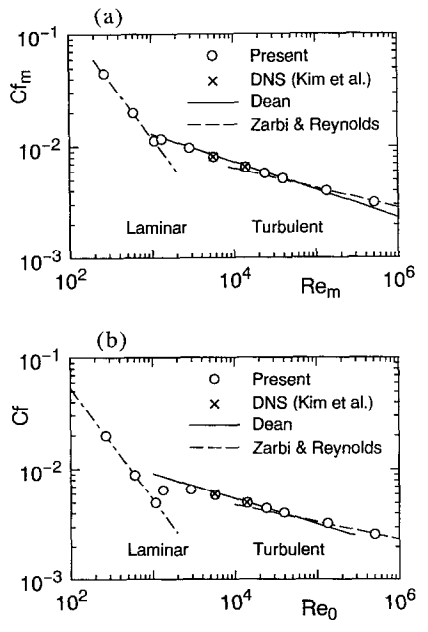

FIG. 2. Friction coefficient of channel flow for various Reynolds numbers: (a) normalized by bulk velocity; (b) normalized by centerline velocity.

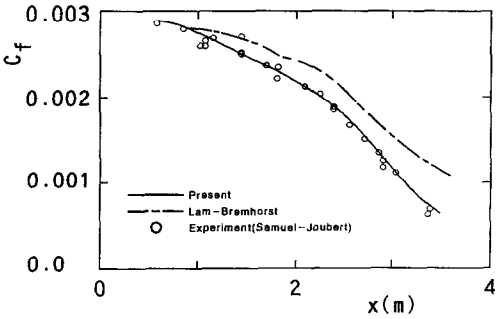

FIG. 3. Friction coefficient of adverse pressure gradient flow.

is conducted with reference to the experiment by Samuel and Joubert [14]. The variation of the skin friction coefficient with a flow development in the streamwise direction is shown in Fig. 3. It can be seen that the present results agree with the experimental data much better than the Lam–Bremhorst model.

The foregoing comparisons demonstrate that the present model can predict quite accurately the attached turbulent flows including the effects of both the Reynolds number and the pressure gradient.

5. APPLICATION TO BACKWARD-FACING STEP FLOWS

5.1. *Numerical procedure and boundary conditions*

In calculating the backward-facing step flow, we used the finite-difference method to discretize the governing equations, employing the third-order upwind difference for the convection term in equation (2), the first-order upwind difference for the convection terms in equations (3) and (4), and the second-order central difference for the other terms. The calculations were performed by the MAC method. The generalized coordinate system was employed and the grid system was non-staggered. Figure 4 shows the present computational grid systems. The finer-resolution grid (Fig. 4(b)) was used to confirm the grid dependence as described later.

The boundary conditions are: $\bar{U} = \bar{V} = k = 0$, $\varepsilon_w = 2\nu k_1/n_1^2$ and $\partial\bar{p}/\partial n = 0$ at the wall surface; $\bar{U}$, $\bar{V}$, k and ε are specified from the experimental conditions together with $\partial^2\bar{p}/\partial n^2 = 0$ at the inlet; and $\partial\bar{U}/\partial x = \partial\bar{V}/\partial x = \partial k/\partial x = \partial\varepsilon/\partial x = 0$ and $\bar{p} = 0$ at the outlet. Some explanations would be appropriate for the boundary conditions of the pressure and the dissipation rate on the wall surface. Strictly, the pressure gradient normal to the wall surface is $\partial\bar{p}/\partial n = \rho\nu(\partial^2\bar{U}_n/\partial n^2)$. The right hand side, however, is known to become almost zero at high Reynolds numbers even in a laminar flow. As described below, we have confirmed the validity of the present boundary condition, $\partial\bar{p}/\partial n = 0$, by comparing the computational results with those obtained with another proper scheme. The strict boundary condition for ε at the wall, on the other hand, is $\varepsilon_w = \nu(\partial^2 k/\partial n^2)$. This type of boundary condition is, however, unstable in the

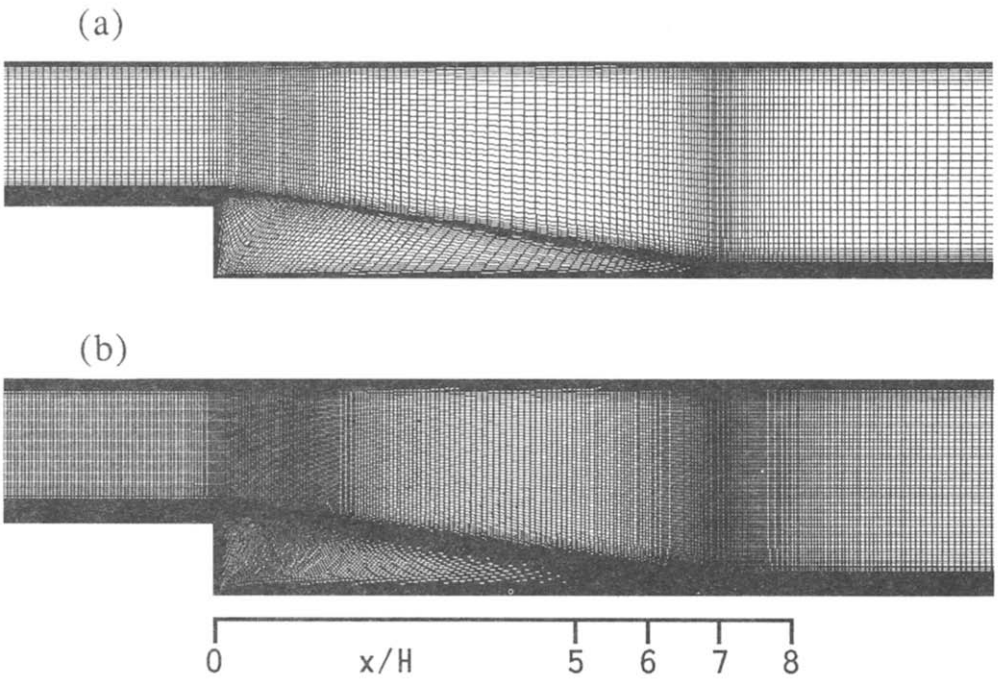

FIG. 4. Grid systems: (a) normal resolution; (b) finer resolution.

initial part of the calculation because the second-order derivative cannot be guaranteed to provide the positive value. Thus, the following conditions are usually employed as the boundary condition for the dissipation rate on the wall surface:

$$\varepsilon_w = 2\nu\left(\frac{\partial\sqrt{k}}{\partial n}\right)^2, \quad \text{or} \quad 2\nu\frac{k_1}{n_1^2}. \tag{18}$$

The validity of the later in equation (18), which is used here, can be shown with the consideration of the near-wall limiting behavior. From equations (11) and (13), the following relation is obtained:

$$2\nu\frac{k}{y^2} = 2\nu\frac{\frac{1}{2}(a_1^2+c_1^2)y^2}{y^2} + \cdots = \nu(a_1^2+c_1^2) = \varepsilon_w \quad \text{for} \quad y \to 0. \tag{19}$$

In this calculation, the grid system is fine enough to reproduce the near-wall limiting behavior, so that the boundary condition with the values k_1 and n_1 at the nearest grid point from the wall as k and y in equation (19) is sufficiently valid.

The calculations were conducted corresponding to six individual experimental cases as shown in Table 1.

5.2. *Evaluation of computational accuracy*

To ascertain the validity of the present calculation, we have performed firstly the calculation of the laminar flow with the grid system shown in Fig. 4(a). The results of the velocity field are presented in Fig. 5. The reattachment length obtained is $X_R/H = 6.43 \pm 0.06$, which is in good agreement with the result of $X_R/H \simeq 6.3$ by Kondoh *et al.* [21]. In the present calculation, the uncertainty in the reattachment length (± 0.06) is approximately equal to the width of the grid spacing near the reattachment point. Furthermore, the center point of the recirculating flow is located at $x/H \simeq 1.85$, $y/H \simeq 0.64$, which is consistent with the result of Kondoh *et al.* [21].

Secondly, we have conducted the turbulent flow calculations corresponding to Case 3 with the two types of grid systems shown in Fig. 4 to evaluate the grid dependence of the computational results. The comparison is shown in Fig. 6, from which we may acknowledge the grid-independent solutions in the calculations.

In addition to the above evaluation, we have carried out the flow calculation corresponding to Case 3 with the scheme developed by Kuno *et al.* [22], in which

Table 1. Computational conditions for back-step flows

Case Data takers	1 Kim [15]	2 Eaton [16]	3 Kasagi [17]	4 Driver [18]	5 Vogel [19]	6 Durst [20]
ER	1.5	1.67	1.5	1.125	1.25	2.0
Re_H	46000	38000	5500	38000	28000	210000
$Re\theta$	1500	1000	500	6500	3500	8000
θ/H	0.033	0.025	0.087	0.17	0.12	0.037
$N_x \times N_y$	211×101	229×101	255×75	207×125	219×125	279×125

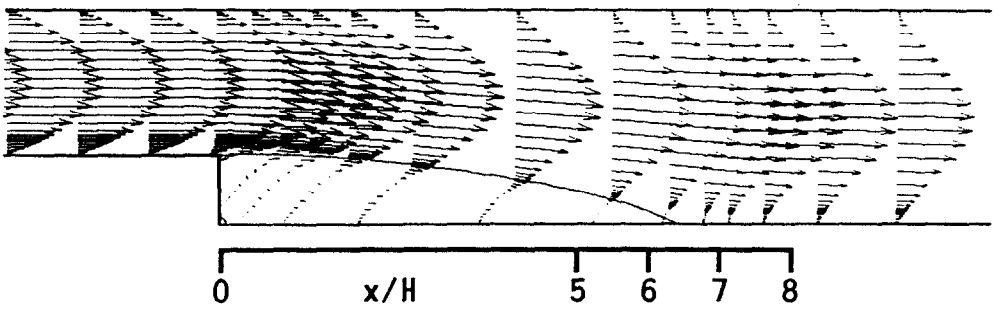

FIG. 5. Overview of velocity field in laminar flow ($ER = 1.5$, $Re_H = 150$).

only the pressure is located in a staggered manner and the relevant pressure boundary condition is properly taken into account. The comparison of the computational results with two types of schemes is also included in Fig. 6, from which one can see that the results are identical with each other and the present calculation procedure based on the MAC method with the $\partial\bar{p}/\partial n = 0$ pressure boundary condition at the wall is valid.

These results assure that the present computations are sufficiently reliable.

6. RESULTS AND DISCUSSION

The predictions of flow reattachment lengths X_R/H for six test cases are compared with the experiments in Fig. 7 and Table 2. The computational results are seen to be in excellent agreement with the experiments. Note that the experimental value of the reattachment length by Kim *et al.* [15, 23] was originally $(7\pm1)H$, but Avva *et al.* [24] reported a corrected value of $7.6H$ which was derived from the pressure distribution on the wall [25]. As mentioned previously, the reattachment lengths have been underpredicted by 15–20% with the standard k–ε model. With the present model, however, we can predict the reattachment length very accurately. The streamlines in Cases 1, 2 and 3 are depicted in Fig. 8. In all cases, the secondary recirculation appears near the step corner as is usually observed experimentally. Furthermore, by comparing the streamlines for Cases 1 and 3 (Figs. 8(a) and (c)), we can find the substantial Reynolds-number dependence of the flow reattachment length with the channel expansion ratio fixed. The present model may be the first to predict the Reynolds-number dependence of the flow reattachment length. Figure 7 and Table 2 suggest that the reattachment length generally increases with increasing expansion ratio except in

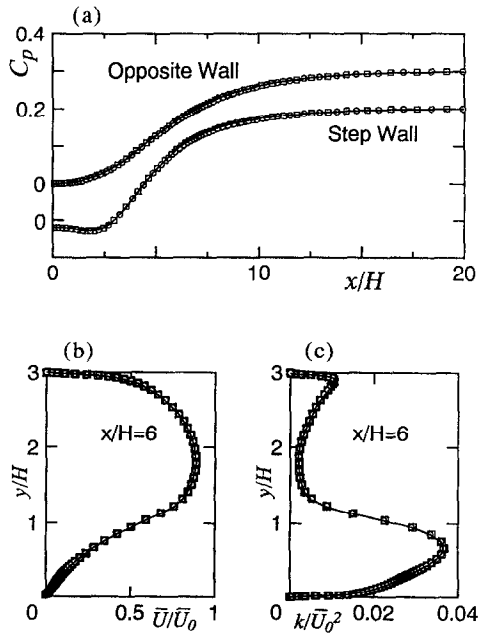

FIG. 6. Evaluation of grid and scheme dependence on computational results (Case 3): — 509×149; ○ 255×75; □ another scheme (see ref. [22]); (a) pressure on walls; (b) streamwise velocity; (c) turbulent energy.

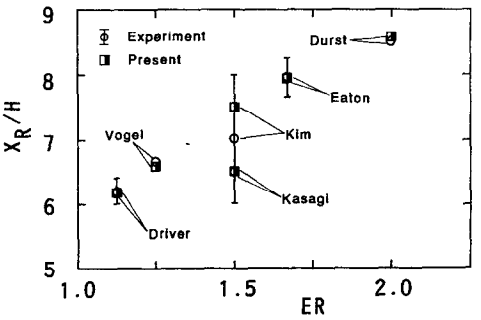

FIG. 7. Comparison of predicted flow reattachment lengths with experiments.

Table 2. Comparison of flow reattachment lengths, X_R/H

Case	1	2	3
Present	7.51±0.03	7.94±0.03	6.52±0.04
Experiment	7±1	7.95	6.51
Case	**4**	**5**	**6**
Present	6.18±0.06	6.59±0.04	8.57±0.04
Experiment	6.21	6.67	8.36

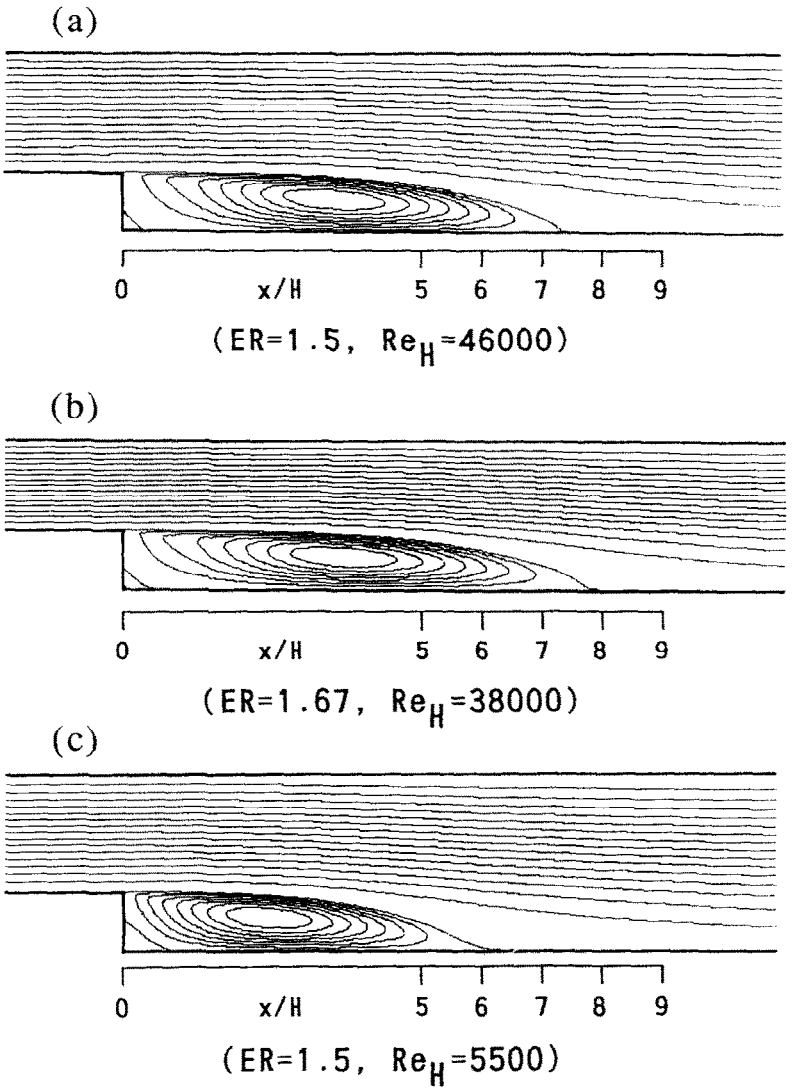

FIG. 8. Streamlines: (a) Case 1; (b) Case 2; (c) Case 3.

the low Reynolds number case. This trend was also indicated experimentally by Eaton and Johnston [26]. The separating streamline and the line of zero streamwise velocity for Case 6 are shown in Fig. 9, compared with the experimental data by Durst and Schmitt [20]. Both of them show almost perfect agreement with the experiment, which means that the present computational results capture the overall flow patterns in the recirculating region very well.

The pressure coefficients on the upper and lower walls in Cases 1 and 2 are presented in Fig. 10. Again, the computational results are seen to agree well with the experiments.

Figures 11 and 12 show the comparisons of the detailed flow field with the experiments of Cases 2 and 3. Case 2 by Eaton and Johnston [16] is regarded as the representative experiment on a backward-facing step flow. And Case 3 by Kasagi *et al.* [17] is regarded as having very small measurement uncertainty and

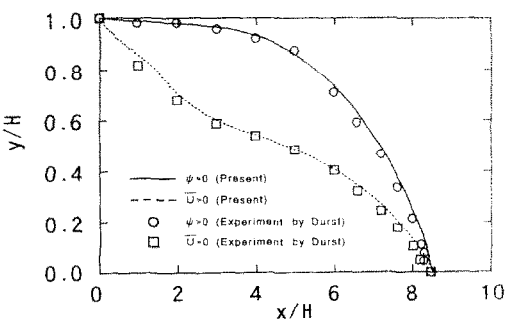

FIG. 9. Comparison of flow pattern in recirculating region: dividing streamline $\psi = 0$ and trace of the point of zero streamwise velocity $\bar{U} = 0$.

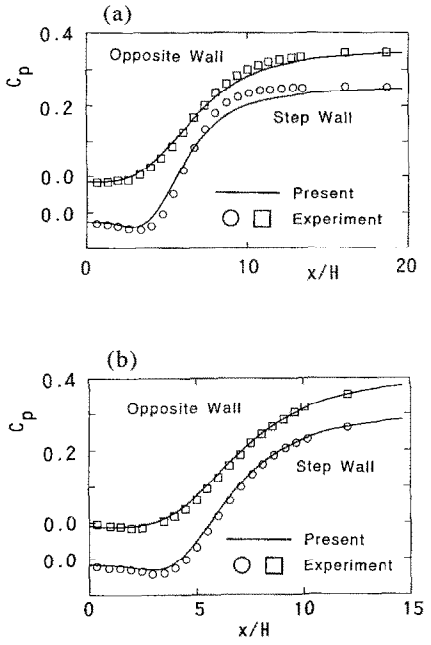

FIG. 10. Pressure coefficient on walls: (a) Case 1; (b) Case 2.

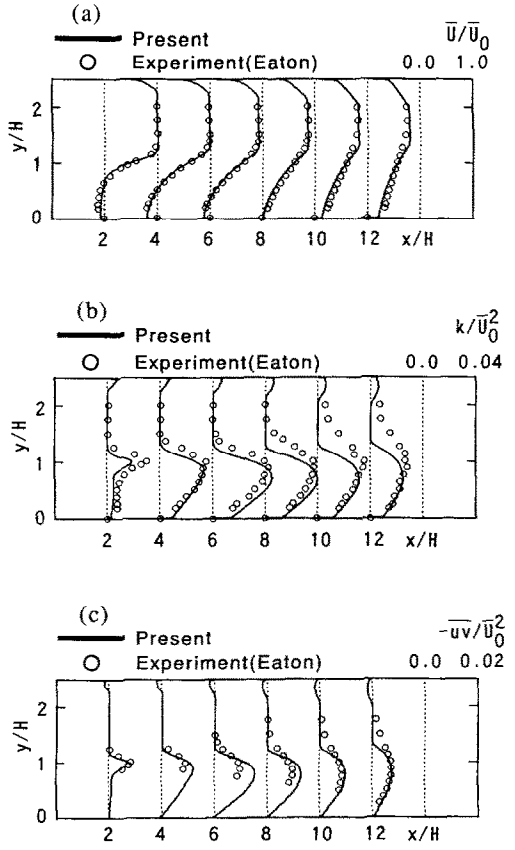

FIG. 11. Comparison with experiment of Eaton *et al.* (Case 2): (a) streamwise velocity; (b) turbulent energy; (c) Reynolds shear stress.

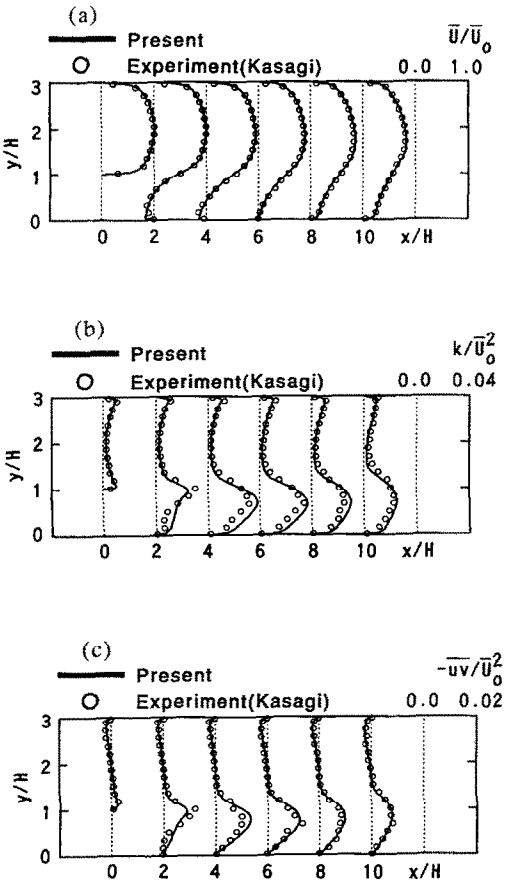

FIG. 12. Comparison with experiment of Kasagi *et al.* (Case 3): (a) streamwise velocity; (b) turbulent energy; (c) Reynolds shear stress.

thus highly reliable. Concerning the streamwise velocity field, the computational results show excellent agreement with the experimental data in both cases. The distributions of the turbulent energy agree reasonably well with the experiments, though there appears a slight difference in the peak locations and in the near-wall values in the recirculating region. As for the Reynolds stress, the computational results of Case 3 conform well to the experiment. The results of Case 2, on the other hand, agree very well with the experimental data in the redeveloping region downstream of the reattachment point; but in the recirculating region they predict a little higher maximums.

The streamwise variations of the local maximums of the streamwise turbulence intensity and the Reynolds shear stress are compared with the experiments in Fig. 13. The computed variations of both quantities are qualitatively consistent with the experiments, in which the absolute maximums occur at a location slightly upstream of the reattachment point. Quantitatively speaking, the computational results of the turbulence intensity in Case 1 agree very well with the experiments, but in the other two cases the present computations give slightly lower values than the exper-

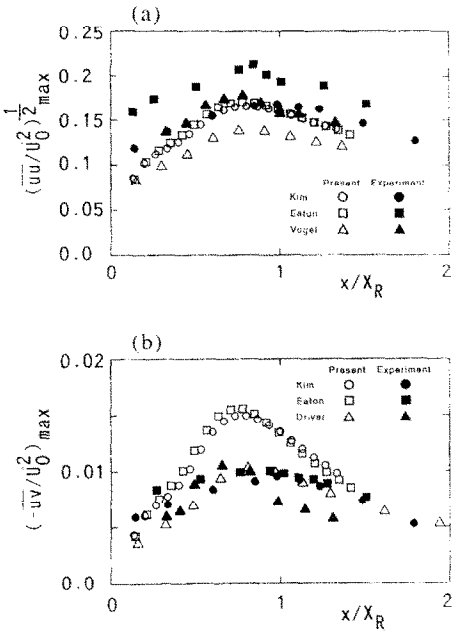

FIG. 13. Streamwise variation of maximum values: (a) streamwise component of turbulent intensity; (b) Reynolds shear stress.

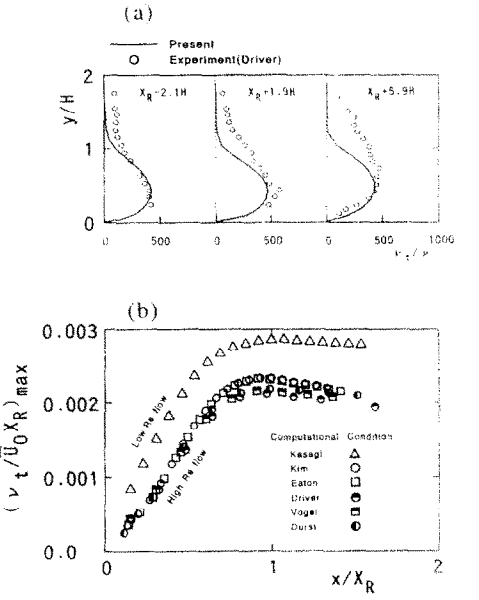

FIG. 14. Distributions of eddy viscosity: (a) comparison with experiment; (b) streamwise variation of local maximums normalized by free stream velocity and reattachment length.

iments, which might be due to the underlying isotropic assumption of the present model. Concerning the Reynolds stress, the computational results show slightly higher values in all cases except Driver's, particularly in the region around and upstream of the reattachment point as seen also in Fig. 11(c).

When predicting the heat transfer in turbulent flows with the k–ε model, a vague concept of the turbulent Prandtl number is usually introduced to express the eddy diffusivity for heat via the eddy viscosity. To avoid this questionable assumption, two-equation heat transfer models have been developed by Nagano *et al.* [27, 28], in which as a natural consequence the eddy viscosity is used as one of the fundamental parameters in determining the eddy diffusivity for heat. Thus, for the prediction of complex turbulent heat transfer, we need a more detailed knowledge of eddy viscosity behavior in flows with separation and reattachment. The distributions of the eddy viscosity are shown in Fig. 14. As shown in Fig. 14(a), the computed results globally agree with the experiments (see the peak value and its location). From Fig. 14(b) we can grasp the growth mechanism of the eddy viscosity. The computations show almost the same tendency in all cases: (a) the local maximum of eddy viscosity increases linearly with the distance from the separation point; (b) the growth rate becomes saturated at $x/X_R \simeq 0.7$ due to the interaction of the detached shear layer with the wall surface and to the subsequent blocking effect of the wall; and (c) the eddy viscosity maintains an almost constant value near the reattachment. The eddy viscosity peaks at a location slightly upstream of the flow reattachment point. The experimental analysis of Vogel and Eaton [19] has elucidated that the maximum heat transfer is located slightly upstream of the reattachment point, which should be noted for being completely consistent with the tendency of the calculated eddy viscosity. The maximum eddy viscosity at the reattachment point normalized by the free stream velocity and the reattachment length, $\nu_t/\bar{U}_0 X_R$, has almost the same value of 0.002 in high Reynolds number flows. It is surprising that, in spite of the calculations under a variety of conditions, such a unique trend of the eddy viscosity is found to exist in all cases of Re_H larger than 10^4.

The comparison of the velocity profile developing along the opposite wall in Case 1 is shown in Fig. 15. In the experiment, the wall shear stresses were obtained by the so-called cross plot technique in which the universal log-law was assumed. However, recently, Nagano *et al.* [29] have indicated experimentally that,

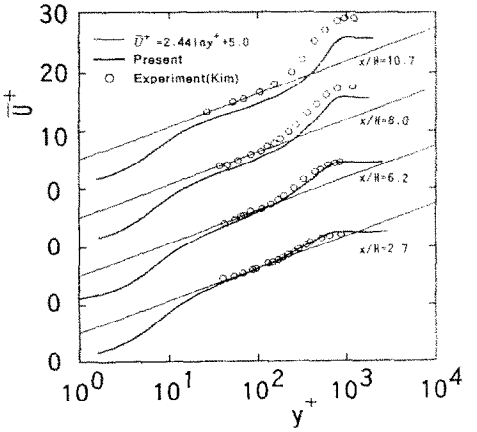

FIG. 15. Mean velocity profiles (Case 1, opposite wall).

under the adverse pressure gradient, the universal log-law is no longer valid and the friction velocity is higher than that obtained by the cross plot technique. The most recent DNS data on the boundary layer flow with an adverse pressure gradient (Spalart and Watmuff [30]) show the same tendency of the friction velocity. Figure 15 indicates that the present computational results are in complete agreement with these latest findings. (Note that the back-step flow is subjected to the strong adverse pressure gradient shown in Fig. 10.)

The flow features in the reverse-flow region are shown in Fig. 16. It can be seen from Fig. 16(a) that the variations of the local maximum of the reverse-flow velocity exhibit almost the same trend in accordance with the experimental data. For the relationship between the Reynolds number and the skin friction coefficient based on the maximum reverse-flow velocity, the computational results give the definite dependency as $-C_f \propto Re_N^{-1/2}$, although slightly higher than in the experiments. In the calculations, the point of the maximum reverse-flow velocity locates closer to the wall than in the experiments, so the calculated friction coefficient becomes larger.

The mean velocity profiles in the recirculating region are presented in Fig. 17, and the mean (C_f) and the fluctuating (C_f') skin friction coefficients along the wall surface are shown in Fig. 18. From Fig. 17, one finds the computed velocities are much smaller than the conventional log-law profile, which qualitatively supports the experiment of Adams and Johnston [31].

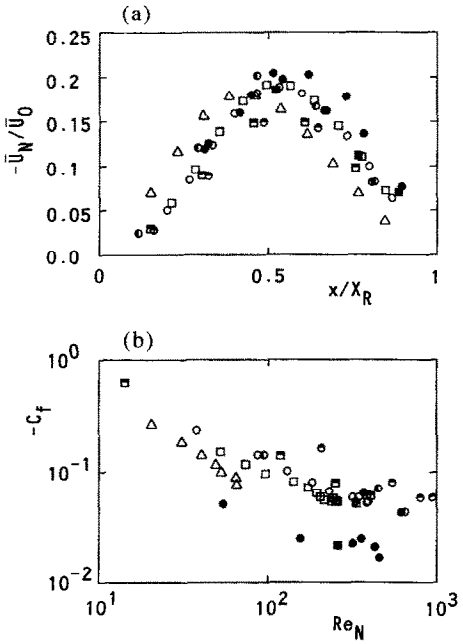

FIG. 16. Flow features in the recirculating region: ○ Case 1; □ Case 2; △ Case 3; ◓ Case 4; ▣ Case 5; ◐ Case 6; ● experiment (Adams); ■ experiment (Eaton); (a) streamwise variation of maximum reverse-flow velocity; (b) relationship between wall-layer Reynolds number Re_N and skin friction coefficient.

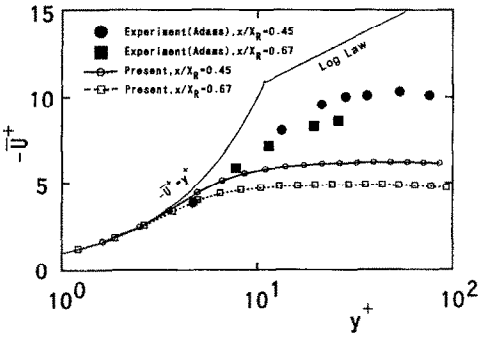

FIG. 17. Mean velocity profiles in recirculating region (computational results correspond to Case 2).

For the skin frictions shown in Fig. 18, the computational results are generally higher than the experimental data of Eaton and Johnston [16]. These discrepancies in Figs. 17 and 18 may be due to the same reason as found in the maximum reverse-flow velocity.

As mentioned previously, the dissipation rate ε on the wall is closely related to the fluctuating friction coefficient C_f'. Considering the near-wall limiting behavior, the following relation can be derived:

$$\varepsilon_w = \nu(\overline{a_1^2}+\overline{c_1^2}) = \nu\frac{\overline{a_1^2}}{b_{11}+\frac{1}{3}} \tag{20}$$

where b_{11} is the streamwise anisotropic tensor. From this relation and equation (12), C_f' is expressed in terms of ε and b_{11} as follows:

$$C_f' = \frac{\rho\sqrt{((b_{11}+\frac{1}{3})\nu\varepsilon_w)}}{\frac{1}{2}\rho\bar{U}_0^2}. \tag{21}$$

Now, as the first estimation, assuming $b_{11} \simeq 0.5$ based on the channel flow data ($\sqrt{\overline{a_1^2}} \simeq 2\sqrt{\overline{c_1^2}}$), we can calculate C_f' from the computational results. The present crude estimation shown in Fig. 18 is higher than in the experiments of Eaton *et al.* However, as indicated by Kasagi *et al.* [17], b_{11} can become smaller than b_{33} near the reattachment point, so that the calculated C_f' will coincide with the experimental level. Additionally, it is worth noting that the variation of C_f' is very similar to that of the Nusselt (or Stanton) number shown by Vogel and Eaton [19]. A concrete discussion on this correlation will be given in a following report.

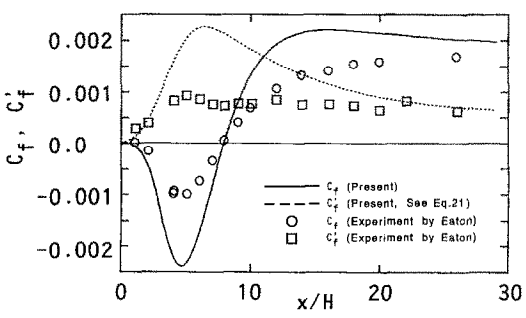

FIG. 18. Mean and fluctuating skin friction coefficients on step wall (Case 2).

7. CONCLUDING REMARKS

We have proposed an improved model of a low-Reynolds-number k-ε model where $u_\tau = (\nu\varepsilon)^{1/4}$ is introduced as the velocity scale of turbulence. We have also reevaluated the model constants so that both attached and separated wall shear flows can be predicted accurately.

As a result of these modifications, the mean flows and turbulent quantities of a backward-facing step flow were predicted quite successfully. The calculated flow reattachment length in particular showed excellent agreement with the measurements for a variety of experimental conditions.

Furthermore, we investigated the detailed aspects of the backward-facing step flow from the computational results, and obtained the following flow structure: (1) the streamwise variation of the eddy viscosity normalized by the free stream velocity and the reattachment length shows almost the same tendency at high Reynolds numbers. (2) The velocity profiles along the opposite wall deviate from the standard log-law in the reattachment region, which is mainly due to the presence of an adverse pressure gradient in a separating and reattaching flow. (3) With the information of the anisotropic tensor b_{ij}, the fluctuating friction coefficient C_f' on the wall can be estimated.

We have also elucidated several flow features which are closely related to the heat transfer in separating and reattaching flows. In particular, it should be mentioned that a knowledge of the growth mechanism of the eddy viscosity is very important to predict the thermal field near a reattachment point where the heat transfer coefficient becomes maximum.

REFERENCES

1. B. E. Launder, On the computation of convective heat transfer in complex turbulent flows, *J. Heat Transfer* **110,** 1112–1128 (1988).
2. M. Ciofalo and M. W. Collins, k-ε predictions of heat transfer in turbulent recirculating flows using an improved wall treatment, *Numer. Heat Transfer B* **15,** 21–47 (1989).
3. N. Djilali, I. Gartshore and M. Salcudean, Calculation of convective heat transfer in recirculating turbulent flow using various near-wall turbulence models, *Numer. Heat Transfer A* **16,** 189–212 (1989).
4. C. G. Speziale, Analytical methods for the development of Reynolds stress closures in turbulence, *Ann. Rev. Fluid Mech.* **23,** 107–157 (1991).
5. S. Thangam and C. G. Speziale, Turbulent flow past a backward-facing step: A critical evaluation of two-equation models, *AIAA J.* **30,** 1314–1320 (1992).
6. S. Nešić and J. Postlethwaite, Calculation of wall-mass transfer rates in separated aqueous flow using a low Reynolds number k-ε model, *Int. J. Heat Mass Transfer* **35,** 1977–1985 (1992).
7. C. K. G. Lam and K. Bremhorst, A modified form of the k-ε model for predicting wall turbulence, *J. Fluids Engng* **103,** 456–460 (1981).
8. Y. Nagano, M. Tagawa and M. Niimi, An improvement of the k-ε turbulence model (the limiting behavior of wall and free turbulence, and the effect of adverse pressure gradient), *JSME J. Ser. B* **55,** 1008–1015 (1989).
9. Y. Nagano and M. Tagawa, An improved k-ε model for boundary layer flows, *J. Fluids Engng* **112,** 33–39 (1990).
10. C. Zhang and A. C. M. Sousa, Numerical simulation of turbulent shear flow in an isothermal heat exchanger model, *J. Fluids Engng* **112,** 48–55 (1990).
11. Y. Nagano and M. Hishida, Improved form of the k-ε model for wall turbulent shear flows, *J. Fluids Engng* **109,** 156–160 (1987).
12. R. K. Avva, S. J. Kline and J. H. Ferziger, Computation of turbulent flow over a backward-facing step—Zonal approach, AIAA-88-0611 (1988).
13. J. Kim *et al.*, The collaborative testing of turbulence models (Organized by P. Bradshaw *et al.*), Data disk No. 4 (1990).
14. A. E. Samuel and P. N. Joubert, A boundary layer developing in an increasingly adverse pressure gradient, *J. Fluid Mech.* **66,** 481–505 (1974).
15. J. Kim, S. J. Kline and J. P. Johnston, Investigation of separation and reattachment of a turbulent shear layer: flow over a backward-facing step, *MD*-37, Thermosciences Division, Department of Mechanical Engineering, Stanford University (1978).
16. J. K. Eaton and J. P. Johnston, Turbulent flow reattachment: an experimental study of the flow and structure behind a backward-facing step, *MD*-39, Thermosciences Division, Department of Mechanical Engineering, Stanford University (1980).
17. N. Kasagi, S. Kawara and A. Matsunaga, Turbulence measurement in a separated and reattaching flow over a backward-facing step with the aid of three-dimensional particle tracking velocimetry, *The Symposium of the Society of Instrument and Control Engineers* (1991).
18. D. M. Driver and H. L. Seegmiller, Features of a reattaching turbulent shear layer in divergent channel flow, *AIAA J.* **23,** 163–171 (1985).
19. J. C. Vogel and J. K. Eaton, Combined heat transfer and fluid dynamic measurements downstream of a backward-facing step, *J. Heat Transfer* **107,** 922–929 (1985).
20. F. Durst and F. Schmitt, Experimental studies of high Reynolds number backward-facing step flow, *Proceedings of 5th Symposium on Turbulent Shear Flows*, pp. 5.19–5.24 (1985).
21. T. Kondoh, Y. Nagano and T. Tsuji, Computational study of laminar heat transfer downstream of a backward-facing step, *Int. J. Heat Mass Transfer* **36,** 577–591 (1993).
22. T. Kuno, N. Satofuka and H. Tokunaga, Numerical solution of incompressible flow of power-law fluid using boundary-fitted curvilinear coordinates, *JSME J. Ser. B* **58,** 2442–2448 (1992).
23. J. Kim, S. J. Kline and J. P. Johnston, Investigation of a reattaching turbulent shear layer: flow over a backward-facing step, *J. Fluids Engng* **102,** 302–308 (1980).
24. R. K. Avva, S. J. Kline and J. H. Ferziger, Computation of the turbulent flow over a backward-facing step using the zonal modeling approach, *TF*-33, Thermosciences Division, Department of Mechanical Engineering, Stanford University (1988).
25. S. Obi and M. Peric, Second-moment calculation procedure for turbulent flows with collocated variable arrangement, *AIAA J.* **29,** 585–590 (1991).
26. J. K. Eaton and J. P. Johnston, A review of research on subsonic turbulent flow reattachment, *AIAA J.* **19,** 1093–1100 (1981).
27. Y. Nagano and C. Kim, A two-equation model for heat transport in wall turbulent shear flows, *J. Heat Transfer* **110,** 583–589 (1988).
28. Y. Nagano, M. Tagawa and T. Tsuji, An improved two-equation heat transfer model for wall turbulent shear flows, *Proc. ASME/JSME Thermal Engng Joint Conference* (Edited by J. Lloyd and Y. Kurosaki), Vol. 3, pp. 233–240 (1991).

29. Y. Nagano, M. Tagawa and T. Tsuji, Effects of adverse pressure gradients on mean flows and turbulence statistics in a boundary layer. In *Turbulent Shear Flows* 8 (Edited by F. Durst *et al.*), pp. 7–21. Springer, Berlin (1993).
30. P. R. Spalart and J. H. Watmuff, Experimental and numerical study of a turbulent boundary layer with pressure gradients, *J. Fluid Mech.* **249,** 337–371 (1993).
31. E. W. Adams and J. P. Johnston, Flow structure in the near-wall zone of a turbulent separated flow, *AIAA J.* **26,** 932–939 (1988).